Evaluation of the Dispersion Diagram of Inhomogeneous Waveguides by the Variational Meshless Method

Vincenzo Lombardi, *Student Member, IEEE*, Maurizio Bozzi, *Fellow, IEEE*, and Luca Perregrini, *Fellow, IEEE*

***Abstract*—This paper presents an extension of the Variational Meshless Method to the calculation of the dispersion diagram of metallic waveguides including inhomogeneous dielectric regions. The method is based on the combination of the variational formulation of a two-dimensional boundary problem and of the meshless method using radial basis functions. The problem requires a vector representation of the field, and it leads to a well-conditioned, real and symmetric eigenproblem, where the matrices depends on the propagation constant β. By solving the eigenproblem for several values of β, a spurious-free dispersion diagram of the guiding structure is obtained. Several structures are studied to demonstrate the accuracy and reliability of the proposed technique. The simulation results are compared with analytical ones, when available, and with those given by a commercial FEM code, always showing a very good agreement with a smaller number of unknowns.**

***Index Terms*—Dispersion diagram, eigenproblem, meshless method, radial basis functions, variational method, waveguide modes.**

I. Introduction

DURING THE LAST DECADE, the scientific community has given a lot of attention to the Meshless Method with Radial Basis Functions (RBFs) [1]–[3]. This technique has been applied to various kind of physical problems such as mechanical, fluid-dynamic, astrophysics and others cases [4]. This technique has also been applied to various classes of electromagnetic problems, e.g. FDTD [5]–[12], boundary problems [13], scattering and imaging problems [14]–[16], inverse-scattering [17], [18], and 2D-eigenvalue problems [19]–[27].

The principal advantage of the Meshless Methods is that they do not require the mesh generation over the domain under study, which is discretized with spatial nodes instead of finite elements as in FEM [28]. In fact, the mesh generation is a time and memory consuming process that sometime requires resources comparable with the solution of the problem. This characteristic of the Meshless Methods is advisable, in particular, when including complicated geometries presenting inhomogeneous materials, discontinuities, or corners. In fact, in the case of mesh-dependent basis functions, a good quality of mesh generation is required to avoid a high interpolation error on the solution [28]. Furthermore in the time-varying simulations a frequent re-meshing may be needed. This often happens in inverse scattering processes, where the use of the Meshless Methods seems promising for real-time simulations [17].

In spite of the many advantages, when applied to electromagnetic eigenproblems, the standard Meshless Method based on radial basis functions (RBFs) presents some limitations [20]. In fact, when a unique value of the shape parameter is adopted for all the RBFs, the solution critically depends on the position of the collocation points, in particular on the boundary of the domain under study [20]. Moreover, a low accuracy is observed in the evaluation of the first eigensolution with the Neumann boundary condition [20]. In [26] a very simple and no-time consuming technique has been proposed to overcome these issues, which is based on a randomized definition of the RBFs with a particular statistical distribution of the shape parameter. Another problem of the Meshless Method with RBFs is that, in its original form, based on the Point Matching technique, it leads to a non-symmetric eigenproblem and, sometimes, to singular matrices, thus making the problem potentially ill-conditioned [30]. To overcome this drawback, in [27] the use of the Variational Formulation [28], [31]–[35] in conjunction with the Meshless Method has been proposed for the first time for the solution of homogeneous waveguides. In [27] a novel automatic refinement technique has also been suggested to add unknowns in the regions of the domain where there is a rapid-varying behavior of the solution. This is done keeping the problem well-conditioned after an arbitrary number of cycles, through a local definition of the shape parameters of the RBFs. Furthermore, the algorithm of [27] does not need preconditioning and, for this reason, it is less time-consuming than the standard meshless method.

In this paper, the extension of the Variational Meshless Method to the determination of the dispersion diagram of inhomogeneous guiding structures is proposed and validated. In the case of inhomogeneous structures, as well-known, a scalar representation of the field through the Hertz-Debye potentials is no longer possible as the eigensolutions of the problem are not separable into TE and TM modes [31]. Therefore, a vector representation of the field is necessary [28]. The magnetic field equation is considered, as it was also done for the electromagnetic tomography of biological tissues [18], and each field component is represented by using three different RBFs. The application of the Variational Meshless Method to

Manuscript submitted October 31, 2018; revised January 16, 2019; accepted January 27, 2019. *Corresponding author: Luca Perregrini.*

This paper is an expanded version from the International Conference on Numerical Electromagnetic and Multiphysics Modeling and Optimization, Reykjavik, Iceland, August 8-10.

The authors are with the Department of Electrical, Computer and Biomedical Engineering, University of Pavia, Pavia, Italy (e-mail: vincenzo.lombardi01@universitadipavia.it, maurizio.bozzi@unipv.it, luca.perregrini@unipv.it).

this kind of problem leads to an eigensystem that permits the evaluation of the dispersion characteristic of the first modes. As it will be pointed out, this technique leads to a well-conditioned eigensystem and the number of unknowns needed to represent the solution is significantly lower than the FEM counterpart.

An outline of the method was given in [36], and some examples of its application were also reported in [37]. The aim of this manuscript is to extend over the conference papers by providing a more detailed and comprehensive description of the Variational Meshless Method for inhomogeneous 2D structures. Therefore, the full development of the algorithm is reported, and useful information for its implementation into an efficient computer code are given. Finally, the numerical results, reported to validate the method and to demonstrate its capabilities, are widely discussed, including a convergence analysis and a comparison with both other numerical techniques and theoretical results (when available).

The paper is organized as follows: Section II describes the basic field theory and its meshless approximation. Section III discusses the numerical implementation of the variational formulation of the field, and the embedding of both the divergence and the boundary conditions in the final eigenvalue problem. Finally, Section IV reports and discusses significant numerical examples that permits to appreciate the accuracy and efficiency of the proposed method.

II. Basic Theory

A. Field Equations

Let us consider the inhomogeneous shielded waveguide shown in Fig. 1, where Ω is the cross section and Γ is its boundary. With the aim of calculating the dispersion diagram of the propagating modes, the vector wave equation is imposed for the magnetic field $\vec{H} = \vec{h}(x, y)\, e^{-j\beta z}$. The propagation constant β is set, and the value of the wavenumbers at which the field can propagate are calculated. Since guiding structures bounded by metallic walls are considered in this paper, the electric wall boundary condition must be enforced. Moreover, the divergence-free condition is also enforced to avoid spurious solutions, as widely discussed in [28], [38]. The problem reduces to the following set of equations [28]

$$\nabla \times \left(\frac{1}{\epsilon_r} \nabla \times \vec{H}(x, y, z) \right) - k_0^2 \mu_r \vec{H}(x, y, z) = 0 \quad \text{in } \Omega \quad (1)$$

$$\nabla \cdot \vec{H} = 0 \quad \text{in } \Omega \quad (2)$$

$$\hat{n} \cdot \vec{H}(x, y, z) = 0 \quad \text{on } \Gamma \quad (3)$$

where $k_0 = 2\pi f \sqrt{\mu_0 \epsilon_0}$ is the wavenumber in vacuum, f is the frequency, μ_0 is the vacuum permeability, ϵ_0 is the vacuum permittivity, and $\hat{n}$ is the outward normal on Γ (see Fig. 1). The problem (1) has the following equivalent variational formulation [28]

$$F(\vec{H}) = \frac{1}{2} \int_\Omega \left(\frac{1}{\epsilon_r} \nabla \times \vec{H} \cdot \nabla \times \vec{H} - k_0^2 \mu_r \vec{H} \cdot \vec{H} \right) d\Omega \quad (4)$$

It is noted that all the components of the magnetic field are continuous also in presence of dielectric discontinuities,

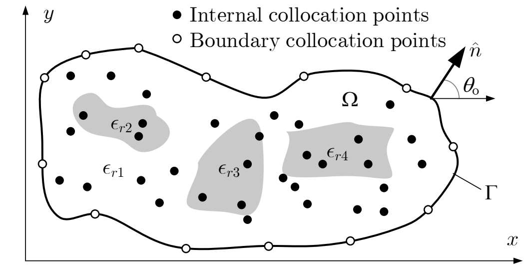

Fig. 1. Geometry of the cross-section of an arbitrarily shaped waveguide including different dielectric materials. The CPs where the RBFs are centered are grouped into internal CPs and boundary CPs.

whereas adopting the equation for the electric field would have also required to enforce the normal field discontinuity at the dielectric interfaces.

To determine the dispersion diagram of the inhomogeneous waveguide, the functional F in (4) must be made stationary. Beside this, the divergence and the boundary condition are also applied.

B. Meshless Approximation

The vector magnetic field can be expressed as

$$\vec{H}(x, y, z) = \left[\hat{x} H^x(x, y) + \hat{y} H^y(x, y) + j \hat{z} H^z(x, y) \right] e^{-j\beta z} \quad (5)$$

It is noted that the z-component of the field is jH^z, as usually done in the variational approach [28]. In this way, the resulting numerical problem will involve only real matrices.

Each component of the field is represented as a combination of RBFs each one centered in a collocation point (CP) (Fig. 1). Calling $h_i^\tau(x, y)$ the RBF centered in the i-th CP, with $\tau = x, y, z$, the component along the direction τ can be written as

$$H^\tau(x, y) = \sum_{i=1}^{N} a_i^\tau h_i^\tau(x, y) \quad (6)$$

It is noted that among the N CPs, there are L internal collocation points (ICPs) that lie within Ω, and M boundary collocation points (BCPs) that lie on Γ, as shown in Fig. 1.

Among the various kinds of RBFs (i.e., Gaussian, multi-quadratic, and inverse quadratic) [1]–[3], in this work Gaussian RBFs are adopted, which are defined as [26]

$$h_i^\tau(x, y) = e^{-\xi_i^\tau c \left[(x - x_i)^2 + (y - y_i)^2 \right]} \quad (7)$$

where (x_i, y_i) is the position of the i-th collocation point. Moreover, the coefficient c is called shape parameter and is related to the width of the function. Its choice is one of the most critical aspects of the meshless methods and can be performed in various manners (see, for instance, [1], [2]). The most common definition is

$$c = 1/(\sigma h^2) \quad (8)$$

where

$$h = \frac{\sqrt{A_\Omega}}{\sqrt{N} - 1} \quad (9)$$

is the average distance between the CPs [12], A_Ω is the total area of the domain Ω, and σ is a parameter typically selected by using preconditioning algorithms, like the leave-one-out cross validation (LOOCV) algorithm [2]. Finally, the parameter ξ_i^τ is a random factor generated for each RBF with a uniform distribution within the interval (0,1). It was introduced in [26] where it was demonstrated its ability to improve the accuracy of the solution. Moreover in [27] it was shown that its use permitted to avoid the time consuming preconditioning step.

It is noted that the Gaussian RBFs (7) are C^∞, and this allows a simple treatment during their differentiation.

III. Numerical Implementation

A. Matrix Representation of the Variational Problem

Substituting (5) and (6) into (4) gives the following functional to extremize

$$F(\boldsymbol{a}) = \frac{1}{2}\left[\boldsymbol{a}^T \boldsymbol{C} \boldsymbol{a} - k^2 \boldsymbol{a}^T \boldsymbol{T} \boldsymbol{a}\right] \tag{10}$$

where

$$\boldsymbol{a} = [a_1^x, a_2^x, \ldots, a_N^x, a_1^y, a_2^y, \ldots, a_N^y, a_1^z, a_2^z, \ldots, a_N^z]^T \tag{11}$$

and

$$\boldsymbol{C} = \begin{bmatrix} \boldsymbol{C}_{11} & \boldsymbol{C}_{12} & \boldsymbol{C}_{13} \\ \boldsymbol{C}_{12}^T & \boldsymbol{C}_{22} & \boldsymbol{C}_{23} \\ \boldsymbol{C}_{13}^T & \boldsymbol{C}_{23}^T & \boldsymbol{C}_{33} \end{bmatrix} \quad \boldsymbol{T} = \begin{bmatrix} \boldsymbol{T}_{11} & \boldsymbol{0} & \boldsymbol{0} \\ \boldsymbol{0} & \boldsymbol{T}_{22} & \boldsymbol{0} \\ \boldsymbol{0} & \boldsymbol{0} & \boldsymbol{T}_{33} \end{bmatrix} \tag{12}$$

The entries of the $N \times N$ sub-matrices $\boldsymbol{C}_{\alpha\beta}$ and $\boldsymbol{T}_{\alpha\beta}$ are given by

$$\begin{aligned}
\boldsymbol{C}_{11}(i,j) &= +\int_\Omega \frac{1}{\epsilon_r}\frac{\partial h_j^x}{\partial y}\ \frac{\partial h_i^x}{\partial y} d\Omega + \beta^2 \int_\Omega \frac{1}{\epsilon_r} h_j^x h_i^x d\Omega \\
\boldsymbol{C}_{22}(i,j) &= +\int_\Omega \frac{1}{\epsilon_r}\frac{\partial h_j^y}{\partial x}\ \frac{\partial h_i^y}{\partial x} d\Omega + \beta^2 \int_\Omega \frac{1}{\epsilon_r} h_j^y h_i^y d\Omega \\
\boldsymbol{C}_{33}(i,j) &= +\int_\Omega \frac{1}{\epsilon_r}\left(\frac{\partial h_j^z}{\partial x}\ \frac{\partial h_i^z}{\partial x} + \frac{\partial h_j^z}{\partial y}\ \frac{\partial h_i^z}{\partial y}\right) d\Omega \\
\boldsymbol{C}_{12}(i,j) &= -\int_\Omega \frac{1}{\epsilon_r}\frac{\partial h_j^x}{\partial y}\ \frac{\partial h_i^y}{\partial x} d\Omega \\
\boldsymbol{C}_{13}(i,j) &= +\beta \int_\Omega \frac{1}{\epsilon_r}\frac{\partial h_j^z}{\partial x}\ h_i^x d\Omega \\
\boldsymbol{C}_{23}(i,j) &= +\beta \int_\Omega \frac{1}{\epsilon_r}\frac{\partial h_j^z}{\partial y}\ h_i^y d\Omega \\
\boldsymbol{T}_{11}(i,j) &= +\int_\Omega \mu_r h_j^x\ h_i^x d\Omega \\
\boldsymbol{T}_{22}(i,j) &= +\int_\Omega \mu_r h_j^y\ h_i^y d\Omega \\
\boldsymbol{T}_{33}(i,j) &= +\int_\Omega \mu_r h_j^z\ h_i^z d\Omega
\end{aligned} \tag{13}$$

where the expressions of the first order derivatives are calculated analytically

$$\begin{aligned}
\frac{\partial h_i^\tau}{\partial x}(x,y) &= -2\xi_i^\tau c(x - x_i) h_i^\tau(x,y) \\
\frac{\partial h_i^\tau}{\partial y}(x,y) &= -2\xi_i^\tau c(y - y_i) h_i^\tau(x,y)
\end{aligned} \tag{14}$$

It is worth noting that due to their definitions $\boldsymbol{C}$ and $\boldsymbol{T}$ are real, symmetric, and nonsingular. Moreover, the matrix $\boldsymbol{T}$ is independent on β, whereas the matrix $\boldsymbol{C}$ can be written as

$$\boldsymbol{C} = \boldsymbol{C}_0 + \beta \boldsymbol{C}_1 + \beta^2 \boldsymbol{C}_2 \tag{15}$$

where $\boldsymbol{C}_0$, $\boldsymbol{C}_1$, $\boldsymbol{C}_2$ are also β-independent.

B. Matrix Representation of the Divergence Condition

On substitution of (5) and (6) in (2) the following expression is obtained

$$\nabla \cdot \vec{H} = \sum_{i=1}^N a_i^x \frac{\partial h_i^x}{\partial x} + \sum_{i=1}^N a_i^y \frac{\partial h_i^y}{\partial x} + \beta \sum_{i=1}^N a_i^z h_i^z \tag{16}$$

Applying the Method of Moments (MoM) by using h_j^z as test functions, (16) is transformed into the following matrix equation

$$\boldsymbol{D}\boldsymbol{a} = \boldsymbol{0} \tag{17}$$

where

$$\boldsymbol{D} = \begin{bmatrix} \boldsymbol{D}_{11} & \boldsymbol{D}_{12} & \boldsymbol{D}_{13} \end{bmatrix} \tag{18}$$

and the $\boldsymbol{D}_{\alpha\beta}$ are all $N \times N$ matrices and their entries are

$$\begin{aligned}
\boldsymbol{D}_{11}(i,j) &= \int_\Omega h_j^z\ \frac{\partial h_i^x}{\partial x} d\Omega \\
\boldsymbol{D}_{12}(i,j) &= \int_\Omega h_j^z\ \frac{\partial h_i^y}{\partial y} d\Omega \\
\boldsymbol{D}_{13}(i,j) &= \beta \int_\Omega h_j^z\ h_i^z d\Omega
\end{aligned} \tag{19}$$

It is noted that matrix $\boldsymbol{D}$ has dimension $N \times 3N$, and his *nullity* is $2N$.

For implementation reasons (see Sec. III-E), it is interesting to note that matrix $\boldsymbol{D}$ can be written as

$$\boldsymbol{D} = \boldsymbol{D}_0 + \beta \boldsymbol{D}_1 \tag{20}$$

where $\boldsymbol{D}_0$, and $\boldsymbol{D}_1$ are both β-independent.

C. Matrix Representation of the Boundary Condition

On substitution of (5) and (6) in (3) and by applying the MoM procedure on the boundary Γ (i.e., testing only with h_j^z centered on the BCPs) the following matrix equation is obtained

$$\boldsymbol{B}\boldsymbol{a} = \boldsymbol{0} \tag{21}$$

where

$$\boldsymbol{B} = \begin{bmatrix} \boldsymbol{B}_{11} & \boldsymbol{B}_{12} & \boldsymbol{0} \end{bmatrix} \tag{22}$$

where $\boldsymbol{0}$ is the $M \times N$ null matrix and $\boldsymbol{B}_{\alpha\beta}$ are $M \times N$ matrices, and their expressions are

$$\begin{aligned}
\boldsymbol{B}_{11}(i,j) &= \int_\Gamma \cos(\theta_o) \left[h_j^z(x_o, y_o) h_i^x(x_o, y_o)\right] dl \\
\boldsymbol{B}_{12}(i,j) &= \int_\Gamma \sin(\theta_o) \left[h_j^z(x_o, y_o) h_i^y(x_o, y_o)\right] dl
\end{aligned} \tag{23}$$

where θ_o is the angle between $\hat{n}$ and $\hat{x}$ on the boundary observation point (x_o, y_o) as shown in Fig. 1. Note that the matrix $\boldsymbol{B}$ is β-independent.

D. Assembling the Final Eigenproblem

Due to (17), the solution vector $\boldsymbol{a}$ must lie in the null space of $\boldsymbol{D}$. This condition can be imposed in the following way

$$\boldsymbol{a} = \boldsymbol{E}_D \boldsymbol{x} \tag{24}$$

where $\boldsymbol{x}$ is $2N \times 1$ unknown vector and $\boldsymbol{E}_D$ is a $3N \times 2N$ matrix and is an orthonormal basis for the null space of $\boldsymbol{D}$ obtained from the singular value decomposition.

Substituting (24) in (21) the following expression is obtained

$$\boldsymbol{B}\boldsymbol{E}_D \boldsymbol{x} = \boldsymbol{0} \tag{25}$$

and it is possible to write

$$\boldsymbol{x} = \boldsymbol{E}_B \boldsymbol{z} \tag{26}$$

where $\boldsymbol{z}$ is an unknown vector and $\boldsymbol{E}_B$ is an orthonormal basis for the null space of $\boldsymbol{B}\boldsymbol{E}_D$, obtained from the singular value decomposition. The *rank* of $\boldsymbol{B}$ is M, the dimension of $\boldsymbol{E}_B$ is $2N \times (N + L)$, and $\boldsymbol{z}$ is an $(N + L) \times 1$ vector.

By combining (26) and (24), substituting in (10) and extremizing the resulting expression, the following eigensystem is obtained

$$\boldsymbol{C'}(\beta)\boldsymbol{z} = k_0^2 \boldsymbol{T'}(\beta)\boldsymbol{z} \tag{27}$$

where

$$\begin{aligned} \boldsymbol{C'}(\beta) &= \boldsymbol{E}_B^T \boldsymbol{E}_D^T \boldsymbol{C} \boldsymbol{E}_D \boldsymbol{E}_B \\ \boldsymbol{T'}(\beta) &= \boldsymbol{E}_B^T \boldsymbol{E}_D^T \boldsymbol{T} \boldsymbol{E}_D \boldsymbol{E}_B \end{aligned} \tag{28}$$

Once the eigenproblem (27) is solved, the original unknowns are calculated as

$$\boldsymbol{a} = (\boldsymbol{E}_D \boldsymbol{E}_B)\, \boldsymbol{z} \tag{29}$$

It is worth noting that, due to (13) and to (19), $\boldsymbol{C'}$ and $\boldsymbol{T'}$ depend on the propagation constant β as parameter. From a computational point of view, this does not represent a drawback, since the matrices are built for a given β and (27) is repeatedly solved for different values of β. Moreover, $\boldsymbol{C'}$ and $\boldsymbol{T'}$ are real, symmetric, and nonsingular, thus leading to a well-conditioned eigenproblem [30]. The dimension of the problem (27) is $(N + L)$, which is smaller than the number of original set unknowns $\boldsymbol{a}$.

By setting the value of β, the solution of the problem (27) provides all the modes propagating within the waveguide with that value of β. On the other hand, the pairs $\{\beta, k_0^{(i)}\}$ (and, therefore, $\{\beta, \omega^{(i)}\}$) for plotting the dispersion diagram are obtained.

E. Implementation of the Algorithm

The theory presented in this section has been implemented in a Matlab code and the flowchart of the resulting script is shown in Fig. 2, where Q is the number of β values to compute. In particular the values of β to be considered $(\beta_1, \ldots, \beta_Q)$ are set by the user.

The first step is the definition of the CPs on the domain. This is done by increasing their density in the regions with higher dielectric constant. More in detail, the definition of the average distance h in (8) is locally modified dividing it by a factor $\sqrt{\epsilon_r}$, and new CPs are added following the procedure described in [27].

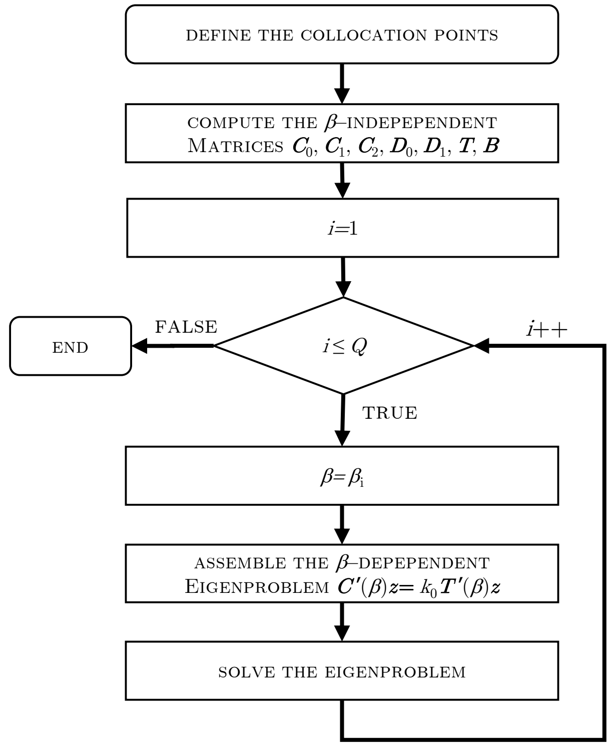

Fig. 2. Flowchart of the implemented algorithm.

In the previous sections it has been noted that the matrices $\boldsymbol{T}$ and $\boldsymbol{B}$, $\boldsymbol{C}_0$, $\boldsymbol{C}_1$, $\boldsymbol{C}_2$, $\boldsymbol{D}_0$, and $\boldsymbol{D}_1$ are β-independent. Therefore, they can be calculated once for all before starting the β-loop, as shown in Fig. 2. After that, the β-loop starts, and the β-dependent matrices $\boldsymbol{C}$, $\boldsymbol{D}$, and $\boldsymbol{E}_D$ are calculated for every value β_i. This permits to assemble the eigenproblem (27) through (28). Its enables permits to compute the wavenumbers of the first modes for that particular value of β. The β-loop stops when all the β values have been considered and the dispersion diagram is plotted.

Since the aim of this work is to demonstrate the accuracy and reliability of the proposed theory, the current implementation of the code is a non-compiled Matlab script, and it does not exploit any geometrical symmetry.

IV. Numerical Results

To demonstrate the performances of the presented method, four examples are reported in this section.

An independent validation is obtained by comparison with analytical results, when available, and with simulation results given by ANSYS HFSS. The code was run on a computer with an Intel Corei7-6700 CPU @ 3.40 GHz (8 CPUs), and 16 GB of RAM.

All the simulations described in the following subsections have been conducted with a fixed value of σ = 1 in (8), in this way it is demonstrated that also in the case of inhomogeneous dielectric filled waveguide the introduction of the parameter ξ_i^τ permits to avoid the preconditioning, as it was proved in [27].

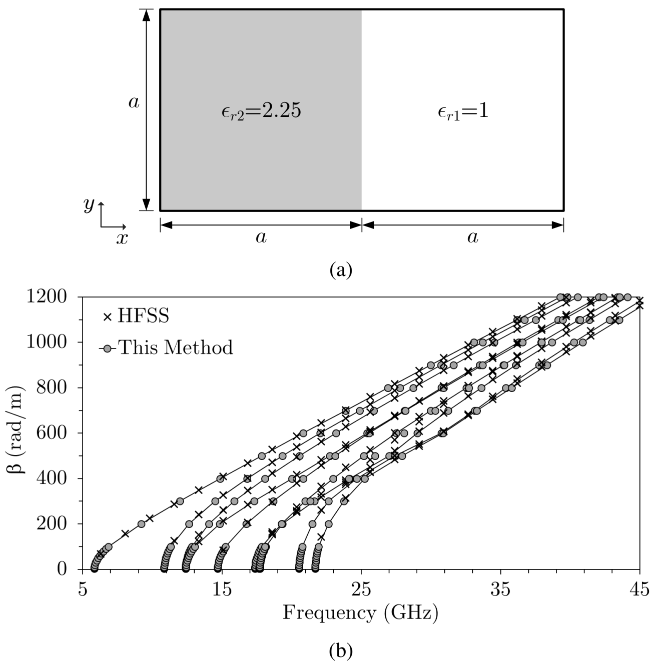

Fig. 3. Dielectric Loaded Waveguide: (a) Geometry of the structure ($a = 10$ mm); (b) Dispersion diagram calculated by the variational meshless method (gray circles) compared with the HFSS simulation (black cross).

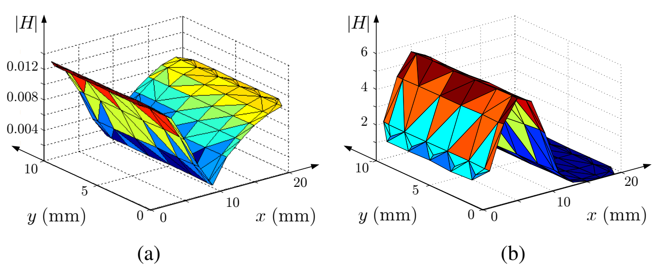

Fig. 4. Behavior of $|\vec{H}|$ (arbitrary units) for the first mode of the Dielectric Loaded Waveguide of Fig. 3: (a) $\beta = 5$ rad/m; (b) $\beta = 1200$ rad/m.

A. Dielectric Loaded Waveguide

The first example refers to the analysis of the dielectric loaded waveguide considered in [39]. The domain is shown in Fig. 3(a), where all the relevant dimensions and information about the dielectric are also provided. The number of collocation points used to define the unknown is $N = 100$ CPs (i.e., $L = 70$ internal CPs and $M = 30$ boundary CPs). In Fig. 3(b) the obtained dispersion diagram is shown and compared with the results given by ANSYS HFSS after a port only simulation with 284 triangles on the input port. The variational meshless method simulation needed overall 1.2 s to compute both the β-independent matrices and the 26 reported β-steps (HFSS CPU time: 26 s). The average discrepancy vs HFSS results was in the order of 1%. It is important to highlight that the presented method has given no spurious solutions.

Beside the dispersion diagram, the proposed method permits to calculate also the modal field for a given value of β. Fig. 4 shows the magnetic field $|\vec{H}|$ of the first mode of the dielectric loaded waveguide in the cases $\beta = 5$ rad/m and $\beta = 1200$ rad/m. As expected, increasing the value of β (and, therefore, the frequency), the field becomes more concentrated in the region with the highest dielectric constant.

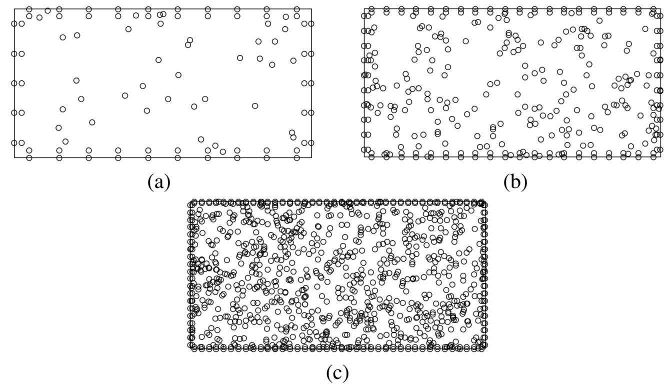

Fig. 5. Random distribution of the CPs used for the convergence analysis of the Dielectric Loaded Waveguide: (a) 100 CPs; (b) 320 CPs; (c) 1040 CPs.

For this structure, an analytical solution is also available [31]. Therefore, it is possible to calculate the error

$$\mathcal{E}(\beta) = \frac{f_{\mathrm{n}}(\beta) - f_{\mathrm{a}}(\beta)}{f_{\mathrm{a}}(\beta)} \tag{30}$$

in the determination of the propagating frequency for a given β. In (30), f_{a} is the analytical value of the frequency [31], and f_{n} is its numerical value calculated by the variational meshless method. This permits to perform a convergence analysis, repeatedly increasing the number of the CPs. Table I reports the results of the convergence analysis for the first mode. The three different random distributions of the CPs shown in Fig. 5) were considered. The errors of the frequency were calculated when β ranges form 0 to 1200 rad/m. It clearly appeared that the error decreased when increasing the number of CPs, and, in the worst case, it is below 0.5% with only 100 CPs.

TABLE I
RELATIVE ERROR IN THE EVALUATION OF THE DISPERSION PAIRS $\{\beta, f\}$ OF THE FIRST MODE OF THE DIELECTRIC LOADED WAVEGUIDE OF FIG. 3. THE RANDOM DISTRIBUTIONS OF THE CPS OF FIG. 5 WERE CONSIDERED.

Propagation constant β (rad/m)	Analytical frequency (GHz)	#CPs = 100 Fig. 5(a) $\mathcal{E}(\beta)$ (%)	#CPs = 320 Fig. 5(b) $\mathcal{E}(\beta)$ (%)	#CPs = 1040 Fig. 5(c) $\mathcal{E}(\beta)$ (%)
0	5.78212	0.4518	0.2919	0.1246
100	6.81088	0.4368	0.2811	0.1273
200	9.14706	0.3937	0.2498	0.1126
300	11.92380	0.3333	0.2072	0.0927
400	14.83090	0.2725	0.1652	0.0728
500	17.79330	0.2218	0.1308	0.0564
600	20.79280	0.1828	0.1051	0.0442
700	23.82170	0.1531	0.0856	0.0350
800	26.87440	0.1300	0.0706	0.0277
900	29.94620	0.1121	0.0592	0.0223
1000	33.03360	0.0978	0.0500	0.0179
1100	36.13360	0.0865	0.0429	0.0145
1200	39.24410	0.0770	0.0370	0.0116

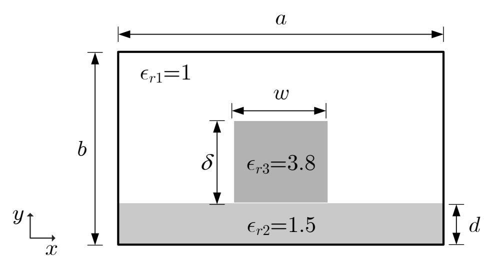

(a)

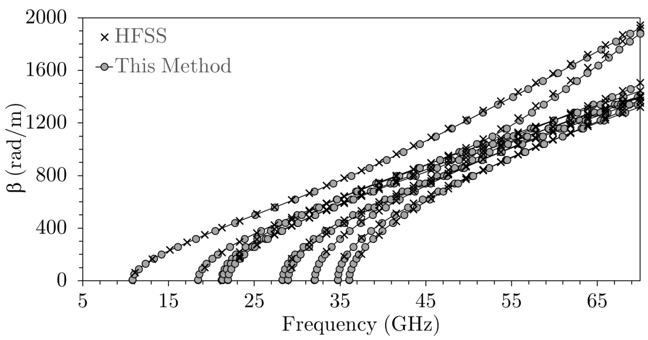

(b)

Fig. 6. Shielded Insulated Image Guide: (a) Geometry of the structure ($\delta = 1$ mm, $w = 2.25$ mm, $d = 0.5$ mm, $a = 13.5$ mm, $b = 8$ mm); (b) Dispersion diagram calculated by the variational meshless method (gray circles) compared with the HFSS simulation (black cross).

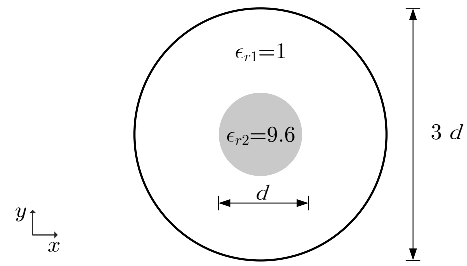

(a)

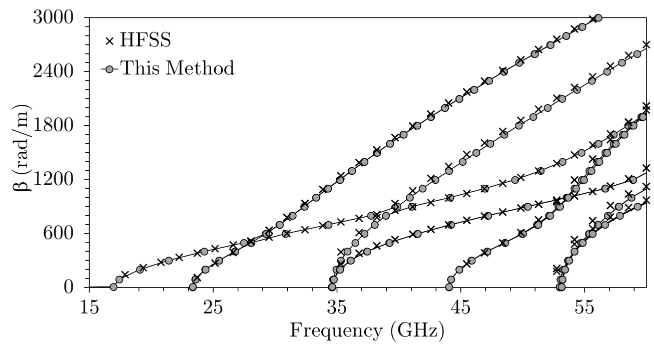

(b)

Fig. 8. Round Double-Layer Shielded Waveguide: (a) Geometry of the structure ($d = 6.35$ mm); (b) Dispersion diagram calculated by the variational meshless method (gray circles) compared with the HFSS simulation (black cross).

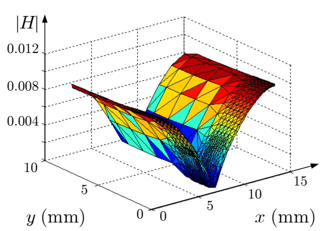

(a)

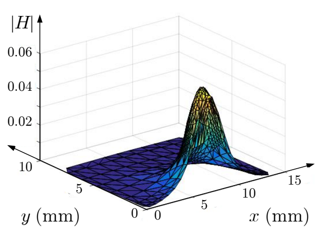

(b)

Fig. 7. Behavior of $|\vec{H}|$ (arbitrary units) for the first mode of the Shielded Insulated Image Guide of Fig. 6: (a) $\beta = 5$ rad/m; (b) $\beta = 1200$ rad/m.

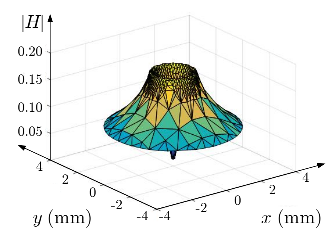

(a)

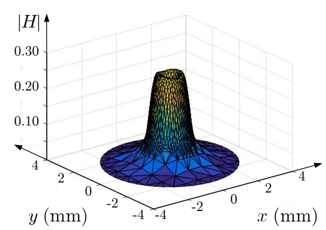

(b)

Fig. 9. Behavior of $|\vec{H}|$ (arbitrary units) for the first mode of the Round Double-Layer Shielded Waveguide of Fig. 8: (a) $\beta = 5$ rad/m; (b) $\beta = 1500$ rad/m.

It is worth noting that by increasing the number of randomly distributed CPs, some of them might tend to coincide (see Fig. 5(c)). Nonetheless, due to the introduction of the random factor ξ_i^τ in (7), as proposed in [26], the RBFs are still independent, and the numerical problem (27) remains well-conditioned [27].

B. Shielded Insulated Image Guide

The second example refers to the analysis of a shielded insulated image waveguide presented in [40]. The domain is shown in Fig. 6(a), where all the relevant dimensions and information about the dielectric are also provided. This is a relevant example to test the proposed method, since it features a multi-dielectric discontinuity (i.e., an edge with three different dielectric materials). The number of collocation points used to define the unknown is $N = 326$ CPs (i.e., $L = 282$ internal CPs and $M = 44$ boundary CPs). In Fig. 6(b) the obtained spurious-free dispersion diagram is shown and compared with the results given by ANSYS HFSS after a port only simulation with 696 triangles on the input port. The simulation with the variational meshless method needed 8.7 s to compute the initial matrices and the reported 37 β-steps (HFSS CPU time: 147 s), and an average discrepancy in the order of 1% was observed.

The magnetic field for two different values of β (namely $\beta = 5$ rad/m and $\beta = 2000$ rad/m) is plotted in Fig. 7, showing the field confinement in the high permittivity dielectric material when the frequency increases.

C. Round Double-Layer Shielded Waveguide

The third example refers to the analysis of a round double-layer shielded waveguide proposed in [41]. The domain is shown in Fig. 8(a), where all the relevant dimensions and information about the dielectric are also provided. As can be easily seen this problem is characterized by a higher discontinuity of the dielectric constant.

To avoid the well-known systematic error due to the representation of circular arcs with discrete nodes, an equivalent external radius of 3.180166 mm has been used in this simula-

TABLE II
RELATIVE ERROR IN THE EVALUATION OF THE DISPERSION PAIRS $\{\beta, f\}$ OF THE FIRST MODE OF THE ROUND DOUBLE-LAYER SHIELDED WAVEGUIDE OF FIG. 8, CONSIDERING 685 CPS.

Propagation constant β (rad/m)	Analytical frequency f (GHz)	Error $\mathcal{E}(\beta)$ (%)
0	16.80500	0.8634
5	16.80650	0.3669
90	17.26530	0.3185
200	18.96420	0.1756
300	21.34080	0.0280
400	24.24910	-0.0994
500	27.48860	-0.1995
900	41.17940	-0.2761
1400	53.09200	-0.1341
1800	58.18670	0.0393

tion, which guarantees the same area for the circular domain and the approximated 45-edges polygonal one.

The number of collocation points used to define the unknown is $N = 685$ CPs (i.e., $L = 640$ internal CPs and $M = 45$ boundary CPs). The simulation needed 42.3 s to compute the initial matrices and the reported 32 cycles. In particular the initial solution, required about 8.0 s, while every cycle lasted about 1.1 s. In Fig. 8(b) the obtained dispersion diagram is shown and compared with the results given by ANSYS HFSS after a port only simulation with 2426 triangles on the input port (HFSS CPU time: 690 s). An average discrepancy in the order of 1% was observed, and, also in this case, the solution was spurious-free.

By increasing the frequency, the field becomes more confined in the dielectric with higher permittivity as shown in Fig. 9 where the cases with $\beta = 5$ rad/m and $\beta = 1500$ rad/m for the first mode are plotted.

This structure has an analytical solution for the dispersion diagram [31], and this allows for calculating the error (30). Table II reports the error in the calculation of the frequency of the first mode, for β ranging form 0 to 1800 rad/m, considering 685 CPs. An error below 1% is observed also in the worst case.

D. Elliptic Inhomogeneous Waveguide

The fourth example refers to the analysis of an elliptic inhomogeneous waveguide proposed in [42]. The domain is shown in Fig. 10(a), where all the relevant dimensions and information about the dielectric are also provided.

The number of collocation points used to define the unknown is $N = 336$ CPs (i.e., $L = 246$ internal CPs and $M = 90$ boundary CPs). The simulation needed 7.44 s to compute the initial matrices and the reported 28 cycles. In particular the initial solution required about 2.9 s, while every cycle lasted about 0.162 s. In Fig. 10(b) the obtained dispersion diagram is shown and compared with the results given by ANSYS HFSS after a port only simulation with 502 triangles on the input port (HFSS CPU time: 112 s). An average discrepancy in the order of 1% was observed, and, also in this case, the solution was spurious-free.

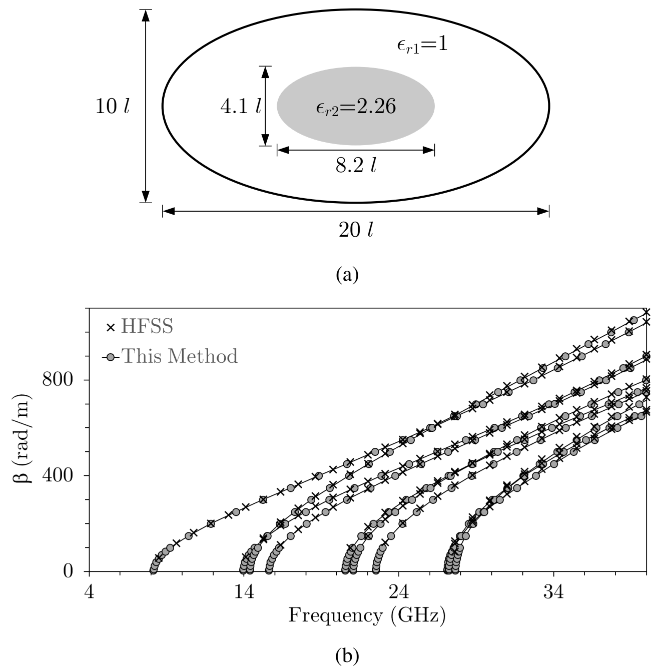

Fig. 10. Elliptic Inhomogeneous Waveguide: (a) Geometry of the structure ($l = 1$ mm); (b) Dispersion diagram calculated by the variational meshless method (gray circles) compared with the HFSS simulation (black cross).

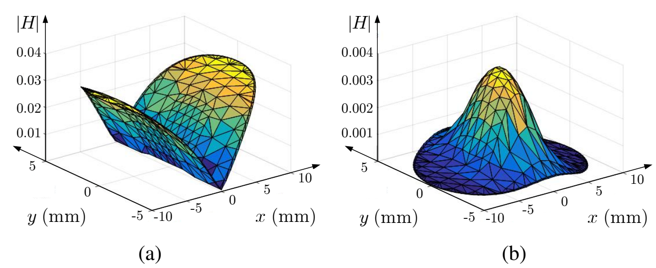

Fig. 11. Behavior of $|\vec{H}|$ (arbitrary units) for the first mode of the Elliptic Inhomogeneous Waveguide of Fig. 10: (a) $\beta = 5$ rad/m; (b) $\beta = 800$ rad/m.

As expected, the increase in frequency leads to the confinement of the field in the dielectric with higher permittivity, as shown in Fig. 11, where the cases with $\beta = 5$ rad/m and $\beta = 800$ rad/m for the first mode are plotted.

V. CONCLUSION

The Variational Meshless Method formerly proposed for homogeneous structures has been extended to simulate inhomogeneous shielded waveguides. To this aim, a vector variational formulation of the electromagnetic problem has been adopted, and the proper boundary condition has been enforced together with the divergence condition. Radial basis functions are defined on randomly defined collocation point in the analysis domain. This leads to a real, symmetric, well-conditioned and spurious-free eigenproblem. A great advantage of the proposed technique is the complete random distribution of the collocation points, which reduces the pre-processing time avoiding the meshing step. Moreover, a good accuracy is achieved with a limited number of unknowns, as it has been proved by the convergence study. The proposed method has been validated through four examples found in the literature, and the results successfully compared with analytical results, when available, and with ANSYS HFSS simulations.

REFERENCES

[1] M. Mongillo, “Choosing basis functions and shape parameters for radial basis function methods,” *SIAM Undergraduate Research Online*, Vol. 4, pp. 190–209, 2011.

[2] B. Fornberg and C. Piret, “On choosing a radial basis function and a shape parameter when solving a convective PDE on a sphere,” *J. Comput. Phys.*, Vol. 227, No. 5, pp. 2758-2780, Feb. 2008.

[3] B. Fornberg, T. A. Driscoll, G. Wrights, and R. Charles, “Observations on the behavior of radial basis function approximations near boundaries,” *Computers & Mathematics with Applications*, Vol. 43, No. 3, pp. 473–490, Feb.–Mar 2002.

[4] G. E. Fasshauer, *Meshfree approximation methods with MATLAB*, Vol. 6, Chicago,: World Scientific, 2007.

[5] Y. Yu and Z. Chen, “A 3-D radial point interpolation method for meshless time-domain modeling,” *IEEE Trans. Microw. Theory Techn.*, Vol. 57, No. 8, pp. 2015–2020, Aug. 2009.

[6] Y. Yu and Z. Chen, “Towards the development of an unconditionally stable time-domain meshless method,” *IEEE Trans. Microw. Theory Techn.*, Vol. 58, No. 3, pp. 578–586, Mar. 2010.

[7] S. Yang, Z. Chen, Y. Yu, and S. Ponomarenko, “A divergence free meshless method based on the vector basis function for transient electromagnetic analysis,” *IEEE Trans. Microw. Theory Techn.*, Vol. 62, No. 7, pp. 1409–1415, Jul. 2014.

[8] S. Yang, Z. Chen, Y. Yu, and S. Ponomarenko, “On the numerical dispersion of the radial point interpolation meshless method,” *IEEE Microw. Compon. Lett*, Vol. 24, No. 10, pp. 653–655, Oct. 2014

[9] T. Kaufmann, C. Fumeaux, and R. Vahldieck, “The meshless radial point interpolation method for time-domain electromagnetics,” in *IEEE MTT-S Int. Microw. Symp. Dig.*, Atlanta, GA, 2008, pp. 61-64

[10] X. Chen, Z. Chen, Y. Yu, and D. Su, “An unconditionally stable radial point interpolation meshless method with Laguerre polynomials,” *IEEE Trans. Antennas Propag.*, Vol. 59, No. 10, pp. 3756-3763, Oct. 2011.

[11] T. Kaufmann, C. Engström, C. Fumeaux, and R. Vahldieck, “Eigenvalue analysis and longtime stability of resonant structures for the meshless radial point interpolation method in time domain,” *IEEE Trans. Microw. Theory Techn.*, Vol. 58, No. 12, pp. 3399–3408, Dec. 2010.

[12] T. Kaufmann, C. Engström, C. Fumeaux, and R. Vahldieck, “Eigenvalue analysis and longtime stability of resonant structures for the meshless radial point interpolation method in time domain,” *IEEE Trans. Microw. Theory Techn.*, Vol. 58, No. 12, pp. 3399–3408, Dec. 2010.

[13] J.-W. Lee and J.-T. Chen, “A semianalytical approach for a nonconfocal suspended strip in an elliptical waveguide,” *IEEE Trans. Microw. Theory Techn.*, Vol. 60, No. 12, pp. 3642–3655, Dec. 2012.

[14] W. L. Nicomedes, R. C. Mesquita, and F. J. d. S. Moreira, ‘’The meshless local Petrov-Galerkin method in two-dimensional electromagnetic wave analysis,” *IEEE Trans. Antennas Propag.*, Vol. 60, No. 4, pp. 1957-1968, Apr. 2012.

[15] M. S. Tong and W. C. Chew, “A novel meshless scheme for solving surface integral equations with flat integral domains,” *IEEE Trans. Antennas Propag.*, Vol. 60, No. 7, pp. 3285-3293, Jul. 2012.

[16] A. Afsari and M. Movahhedi, “An adaptive radial point interpolation meshless method for simulation of electromagnetic and optical fields,” *IEEE Trans. Magn.*, Vol. 50, No. 7, pp. 1–8, Jul. 2014.

[17] M. S. Tong and C. X. Yang, “A meshless method of solving inverse scattering problems for imaging dielectric objects,” *IEEE Trans. Geosci. Remote Sens.*, Vol. 54, No. 2, pp. 990–999, Feb. 2016

[18] A. Afsari, A. M. Abbosh, and Y. Rahmat-Samii, “Modified Born iterative method in medical electromagnetic tomography using magnetic field fluctuation contrast source operator,” *IEEE Trans. Microw. Theory Techn.* Vol. 67 , no. 1, pp. 454-463, Jan. 2019.

[19] S. J. Lai and B. Z. Wang, “Solving Helmholtz equation by meshless radial basis functions method,” *Prog. Electromagn. Res. B*, Vol. 24, pp. 351–367, 2010.

[20] R. B. Platte and T. A. Driscoll, “Computing eigenmodes of elliptic operators using radial basis functions,” *Computers & mathematics with applications*, Vol. 48, No. 3, pp. 561-576, Mar./Apr. 2004.

[21] E. Larsson and B. Fornberg, “A numerical study of some radial basis function based solution methods for elliptic PDEs,” *Computers & Mathematics with Applications*, Vol. 46, No. 5 pp. 891–902, Sep. 2003.

[22] P. Kowalczyk and M. Mrozowski, ”Mesh-free approach to Hemholtz equation based on radial basis functions,” in *15th Int. Conf. Microwaves, Radar and Wireless Communications*, Vol. 2, No. 1719, pp. 702–705, May 2004.

[23] T. Kaufmann, C. Engstrröm, and C. Fumeaux, “Characterization of an adaptive refinement algorithm for a meshless eigenvalue solver based on radial basis functions,” in *IEEE Electromagn. Compat. Symp. (EMC)*, Melbourne, 2010.

[24] T. Kaufmann, C. Engstrröm, and C. Fumeaux, “Adaptive meshless methods in electromagnetic modeling: a gradient-based refinement strategy,” in *41th European Microwave Conference (EuMC2011)*, Manchester, UK, Oct 12-14, 2011.

[25] J. Yu and H. Zhang, “Solving waveguide eigenvalue problem by using radial basis function method,” in *IEEE World Automation Congress*, Hawaii, HI, 2008, pp. 1–5.

[26] V. Lombardi, M. Bozzi, and L. Perregrini, “An improved meshless method for waveguide eigenvalue problems,” *IEEE Microw. Compon. Lett.*, Vol. 27, No. 12, pp. 1047–1049, Dec. 2017

[27] V. Lombardi, M. Bozzi, and L. Perregrini, “A novel variational meshless method with radial basis functions for waveguide eigenvalue problems,” *IEEE Trans. Microw. Theory Techn.*, Vol. 66, No. 8, pp. 3714-3723, Aug. 2017

[28] J. M. Jin, *The finite element method in electromagnetics*, John Wiley & Sons, 2015.

[29] S. M. Rao, D. R. Wilton, and A. W. Glisson, “Electromagnetic scattering by surfaces of arbitrary shape,” *IEEE Trans. Antennas Propag.*, Vol. 30, No. 3, pp. 409–418, May 1982.

[30] J. H. Wilkinson, *The algebraic eigenvalue problem*, Vol. 87, Oxford: Clarendon Press, 1965.

[31] F. R. Harrington, *Time-harmonic electromagnetic fields*, Wiley-IEEE Press, 2001.

[32] A. D. Berk, “Variational principle for electromagnetic resonators and waveguide,” *IRE Trans. Antennas Propag.*, Vol. 4, No. 2, pp. 104-111 ,Apr. 1956.

[33] K. Kurokawa, “Electromagnetic waves in waveguides with wall impedance,” *IEEE Trans. Microw. Theory Techn.*, Vol. 10, No. 5, pp. 314- 320, Sep. 1962.

[34] W. J. English and F. J. Young, “An E-vector variational formulation of Maxwell equations for cylindrical waveguide problems,” *IEEE Trans. Microw. Theory Techn.*, Vol. 19, No. 1, pp. 40-46, Jan. 1971.

[35] M. M. Ilić, A. Ž. Ilić, and B. M. Notaroš, “Efficient Large-Domain 2-D FEM Solution of Arbitrary Waveguides Using p-Refinement on Generalized Quadrilaterals,” *IEEE Trans. Microw. Theory Techn.*, Vol. 53, No. 4, pp. 1377-1383, Apr. 2005.

[36] V. Lombardi, M. Bozzi, L. Perregrini, “Vector Formulation of the Meshless Variational Method for Inhomogeneous Rectangular Waveguides,” *2018 IEEE MTT-S International Conference on Numerical Electromagnetic and Multiphysics Modeling and Optimization (NEMO)*, Reykjavik, 2018, pp. 1-3.

[37] V. Lombardi, M. Bozzi, and L. Perregrini, “Analysis of Inhomogeneous Rectangular Waveguides by the Variational Meshless Method,” *48th European Microwave Conference (EuMC2018)*, Madrid, Spain, 23-28 Sep. 2018.

[38] D. B. Davidson, *Computational Electromagnetics for RF and Microwave Engineering*, Cambridge University Press, 2010.

[39] T. Angkaew, M. Matsuhara, and N. Kumagai, “Finite-element analysis of waveguide modes: a novel approach that eliminates spurious modes,” *IEEE Trans. Microw. Theory Techn.*, Vol. 35, No. 2, pp. 117-123, Feb. 1987.

[40] V. J. Brankovic, D. V. Krupezevic, and F. Arndt, “An efficient two-dimensional graded mesh finite-difference time-domain algorithm for shielded or open waveguide structures, ” *IEEE Trans. Microw. Theory Techn.*, Vol. 40, No. 12, pp. 2272-2277, Mar. 1992.

[41] V. A. Malakhov, V. A. Raevskii, and S. B. Raevskii, “ Added solutions of boundary value problems for double-layer guiding structures, ” *International Journal of Electromagnetics and Applications*, Vol. 5, No. 2, pp. 114-119., 2012.

[42] S. R. Rengarajan and J. E. Lewis, “Dielectric loaded elliptical waveguides,” *IEEE Trans. Microw. Theory Techn.*, Vol. 28, No. 10, pp. 1085-1089, Oct. 1980.

Vincenzo Lombardi (S'16) was born in Milan, Italy, in 1983. He received the BS degree summa cum laude in Electronics and Telecommunications Engineering from the University of Pavia in July 2005 working on the modeling of the losses the HFSS and the implementation of this calculus in a simulator based on the BI-RME method. He received the Master degree in Electronic Engineering in 2007 summa cum laude at the University of Pavia working on the non-linear signaling and time-variant systems and their mathematical modeling focusing on a mixer for wireless receiver in CMOS technology.

In 2014 he joined the University of Pavia as guest researcher, and as PhD student from October 2016. During this activity he is working about mathematical modeling and scientific computing of microwave systems. His current research interest is focused on the development of efficient numerical algorithms for computational electromagnetic, including the Meshless Method with Radial Basis Functions and the BI-RME method.

Maurizio Bozzi (S'98-M'01-SM'12-F'18) was born in Voghera, Italy, in 1971. He received the Ph.D. degree in electronics and computer science from the University of Pavia, Pavia, Italy, in 2000.

He held research positions with various universities worldwide, including the Technische Universität Darmstadt, Germany; the Universitat de Valencia, Spain; and the École Polytechnique de Montréal, Canada. In 2002, he joined the Department of Electronics, University of Pavia, where he is currently an Associate Professor of electromagnetic fields (with Full Professor habilitation). He was also a Guest Professor at Tianjin University, China (2015-2017) and a Visiting Professor at Gdansk University of Technology, Poland (2017-2018).

He has authored or co-authored more than 120 journal papers and 300 conference papers. He co-edited the book *Periodic Structures* (Res. Signpost, 2006) and co-authored the book *Microstrip Lines and Slotlines* (Artech House, 2013). His main research interests concern the computational electromagnetics, the substrate integrated waveguide technology, and the use of novel materials and fabrication technologies for microwave circuits (including paper, textile, and 3D printing).

Prof. Bozzi is an Elected Member of the Administrative Committee of the IEEE Microwave Theory and Techniques Society (MTT-S) for term 2017-2019. He is the Chair of the Meeting and Symposia Committee of the IEEE MTT-S AdCom for years 2018-2019. He was the Secretary of the IEEE MTT-S for year 2016 and a member of the General Assembly (GA) of the European Microwave Association (EuMA) from 2014 to 2016. He was an associate editor of IEEE Microwave and Wireless Components Letters, the *IET Electronics Letters*, and the *IET Microwaves, Antennas and Propagation*. He was the Guest Editor of special issues in the IEEE Transactions on Microwave Theory and Techniques, the IEEE Microwave Magazine, and the *IET Microwaves, Antennas and Propagation*. He was the General Chair of the IEEE MTT-S International Microwave Workshop Series-Advanced Materials and Processes (IMWS-AMP 2017), in Pavia, Italy, 2017, of the IEEE International Conference on Numerical Electromagnetic Modeling and Optimization (NEMO2014), in Pavia, Italy, 2014, and of the IEEE MTT-S International Microwave Workshop Series on Millimeter Wave Integration Technologies, in Sitges, Spain, 2011. He received several awards, including the 2015 Premium Award for Best Paper in IET Microwaves, Antennas & Propagation, the 2014 Premium Award for the Best Paper in Electronics Letters, the Best Student Paper Award at the 2016 IEEE Topical Conference on Wireless Sensors and Sensor Networks (WiSNet2016), the Best Paper Award at the 15th Mediterranean Microwave Symposium (MMS2015), the Best Student Award at the 4th European Conference on Antennas and Propagation (EuCAP 2010), the Best Young Scientist Paper Award of the XXVII General Assembly of URSI in 2002, and the MECSA Prize of the Italian Conference on Electromagnetics (XIII RiNEm), in 2000.

Luca Perregrini (M'97-SM'12-F'16) was born in Sondrio, Italy, in 1964. He received the Laurea degree in electronic engineering and Ph.D. degree in electronics and computer science in 1989 and 1993, respectively.

In 1992, he joined the Faculty of Engineering, University of Pavia, Pavia, Italy, where he is currently a Full Professor of electromagnetic fields and responsible for the Microwave Laboratory. He was a Visiting Professor with the École Polytechnique de Montréal, QC, Canada, in 2001, 2002, 2005, and 2006. He has been responsible for many research contracts with prominent international research centers and companies. He has authored or co-authored over 100 journal papers and over 300 conference papers, 6 book chapters, and 2 textbooks, and co-edited *Periodic Structures* (Res. Signpost, 2006). His current research interests include the development of numerical methods for electromagnetics and the design of microwave components and antennas.

Dr. Perregrini was a member of the General Assembly of the European Microwave Association (EuMA) from 2011 to 2013. He served as a member of Prize Committees for several conferences/societies. He is a member of the Technical Committee MTT-15 (Microwave Field Theory) of the IEEE Microwave Theory and Technique Society (MTT-S) and the Board of Directors of EuMA. He was the co-recipient of several Best Paper Awards at international conferences. He was the Technical Program Committee Chair of the International Microwave Workshop Series on Advanced Materials and Processes, Pavia, Italy, in 2017, of the IEEE MTT-S International Conference on Numerical Electromagnetic Modeling and Optimization, Pavia, in 2014, and of the European Microwave Conference, Rome, Italy, in 2014. He has been an invited speaker at many conferences, and has delivered invited seminar talks at universities and research centers worldwide. He was an Associate Editor of IEEE Microwave and Wireless Components Letters from 2010 to 2013, the IEEE Transactions on Microwave Theory and Techniques from 2013 to 2016, the *International Journal of Microwave and Wireless Technologies* from 2011 to 2016, and *IET Electronic Letters* from 2015 to 2016. He was a Guest Editor of the IEEE Transactions on Microwave Theory and Techniques in 2015 and the *International Journal of Microwave and Wireless Technologies* in 2015. He is currently the Editor-in-Chief of the IEEE Transactions on Microwave Theory and Techniques.